Cell Metabolism
Resource

^{13}C-Pyruvate Imaging Reveals Alterations in Glycolysis that Precede c-*Myc*-Induced Tumor Formation and Regression

Simon Hu,[1,5] Asha Balakrishnan,[2,5] Robert A. Bok,[1] Brittany Anderton,[2] Peder E.Z. Larson,[1] Sarah J. Nelson,[1] John Kurhanewicz,[1] Daniel B. Vigneron,[1,4,*] and Andrei Goga[2,3,4,*]
[1]Department of Radiology and Biomedical Imaging
[2]Department of Medicine, Division of Hematology/Oncology
[3]Helen Diller Comprehensive Cancer Center
[4]Liver Center
University of California, San Francisco, San Francisco, CA 94143, USA
[5]These authors contributed equally to this work
*Correspondence: dan.vigneron@ucsf.edu (D.B.V.), andrei.goga@ucsf.edu (A.G.)
DOI 10.1016/j.cmet.2011.04.012

SUMMARY

Tumor cells have an altered metabolic phenotype characterized by increased glycolysis and diminished oxidative phosphorylation. Despite the suspected importance of glycolysis in tumorigenesis, the temporal relationship between oncogene signaling, in vivo tumor formation, and glycolytic pathway activity is poorly understood. Moreover, how glycolytic pathways are altered as tumors regress remains unknown. Here, we use a switchable model of *Myc*-driven liver cancer, along with hyperpolarized ^{13}C-pyruvate magnetic resonance spectroscopic imaging (MRSI) to visualize glycolysis in de novo tumor formation and regression. LDHA abundance and activity in tumors is tightly correlated to in vivo pyruvate conversion to lactate and is rapidly inhibited as tumors begin to regress, as are numerous glycolysis pathway genes. Conversion of pyruvate to alanine predominates in precancerous tissues prior to observable morphologic or histological changes. These results demonstrate that metabolic changes precede tumor formation and regression and are directly linked to the activity of a single oncogene.

INTRODUCTION

Cellular transformation has been correlated with increased aerobic glycolysis and diminished oxidative phosphorylation (Warburg Effect) (Christofk et al., 2008; Dang and Semenza, 1999; Vander Heiden et al., 2009; Warburg, 1956). Increased glycolysis may contribute both to energy production and the generation of metabolic intermediates that sustain anabolic processes required for rapid tumor growth (Vander Heiden et al., 2009). Lactate dehydrogenase A (*Ldha*) is a key regulator of glycolysis, and its inhibition can attenuate the growth of transplanted tumor cells (Fantin et al., 2006; Le et al., 2010). We sought to determine whether glycolytic changes could be detected prior to other pathological alterations. To visualize the temporal connection between oncogene signaling and glycolysis in de novo tumor formation, we used a switchable transgenic model of *Myc*-driven liver cancer (Goga et al., 2007; Shachaf et al., 2004). Double-transgenic LAP-tTA (LT2) × TRE-MYC (MYC) mice (hereafter called LT2/MYC) express the *Myc* oncogene specifically in hepatocytes in a doxycycline-regulated manner and give rise to tumors that have features of human hepatocellular carcinoma and hepatoblastoma (Cairo et al., 2008; Shachaf et al., 2004). This model allows us to examine in vivo glycolytic changes at different stages of liver tumor formation as well as the consequence of acutely inhibiting oncogene signaling in established tumors. Hyperpolarized ^{13}C MRSI, an emerging metabolic imaging modality (Golman et al., 2006; Hu et al., 2010), was used to visualize glycolysis at different stages of de novo tumor formation and regression in LT2/MYC mice. We show that hyperpolarized ^{13}C MRSI can detect metabolic changes during tumor formation as well as when tumors regress. We find that pyruvate to lactate conversion increased as tumors developed and was rapidly inhibited during regression. Numerous glycolysis pathway genes showed a similar expression pattern. Interestingly, conversion of pyruvate to alanine was predominant in very early stages of tumorigenesis, prior to any observable morphologic or histological changes. Changes in gene expression of glutamine and tricarboxylic acid (TCA) cycle pathways was also altered indicating that global metabolic changes occur as tumors form and regress. These results demonstrate that metabolic changes precede tumor formation and regression and are directly linked to the activity of a single oncogene such as *Myc*. Our study further highlights the potential of high alanine levels as an early biomarker for liver tumor development.

RESULTS

Doxycycline-Regulated MYC Expression Precedes Liver Tumor Formation and Is Inhibited During Regression

We first sought to define the different stages of tumorigenesis and regression. Control (LT2) mice and LT2/MYC mice kept

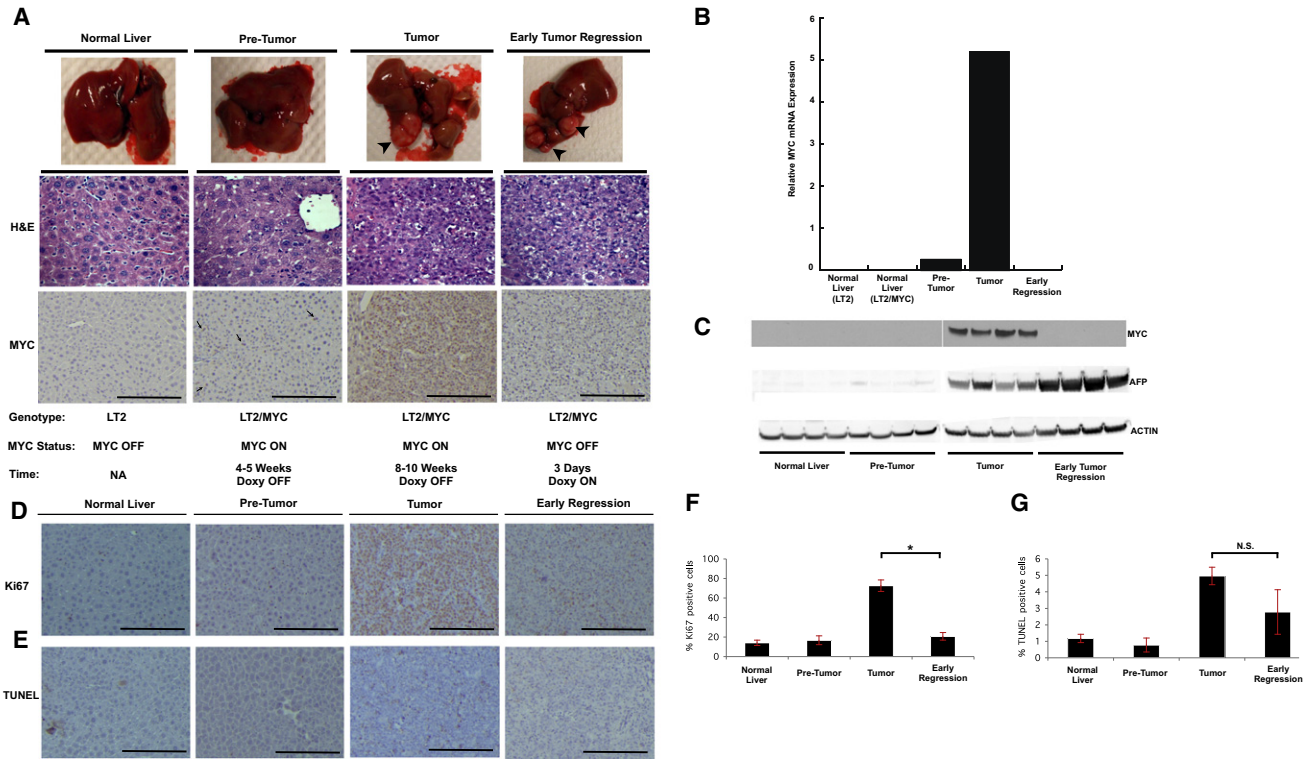

Figure 1. Switchable MYC expression in Primary Liver Tumor Formation and Early Regression

(A) Gross tissues, corresponding histology and MYC staining at different stages of tumor formation and early regression. No apparent histologic differences were noted between primary tumors and early regression sections. MYC expression (indicated with arrowheads) is heterogeneous in pretumor tissue, is significantly increased in tumors, and is absent after 72 hr of doxy treatment.

(B and C) Quantitative PCR (B) and western blots (C) show negligible MYC expression in early-stage pretumor liver compared to elevated expression in established tumors. MYC mRNA and protein expression is switched off when doxy is administered for 3 days. The liver tumor marker, AFP is highly expressed in tumor tissue and persists once MYC is switched off (C).

(D and E) Comparison of staining for the Ki67 proliferation marker (D) and TUNEL assay (E) of liver samples at different stages of tumor development and regression.

(F) Graph depicting percentage of Ki67-positive cells.

(G) Graph depicting percentage of TUNEL-positive cells.

Error bars represent the standard error of the mean (SEM). *$p < 0.004$. N.S., not significant.

continuously on doxycycline (doxy) do not express the *Myc* transgene and do not form tumors (Figures 1A–1C). When doxycycline-containing food is withdrawn from LT2/MYC mice for 4–5 weeks, the *Myc* transgene is modestly induced, but there are no apparent phenotypic or histological changes to indicate tumor formation (Figures 1A–1C). Prolonged removal of doxy for 8–10 weeks results in the formation of discrete tumor nodules, which have features of an aggressive malignancy. LT2/MYC tumors are comprised of small basophilic cells, with a high nuclear to cytoplasmic ratio, frequent mitotic figures indicating high proliferation and occasional apoptotic cells (Figure 1A) (Goga et al., 2007; Shachaf et al., 2004). These tumor nodules are also associated with ~20-fold increased MYC mRNA and protein expression compared to the pretumor liver tissues (Figures 1B and 1C). Immunohistochemical staining for MYC shows a heterogeneous upregulation in a small subset of pretumor liver cells, but a much more dramatic and uniform increased expression in tumor tissues (Figure 1A). This shows that the *Myc* transgene is not uniformly activated in all cells of the mouse liver. This resembles human tumor initiation and progression wherein activation of the driving oncogene may occur in subsets of cells within a tissue.

This model system also allows for inhibition of MYC expression in primary tumors by addition of doxycycline to the mice's diet. Prolonged doxy administration can lead to complete regression of *Myc*-driven liver tumors; however, this takes several weeks (Shachaf et al., 2004) (data not shown). Since we sought to examine the acute metabolic changes that occur once the expression of a driving oncogene such as *Myc* is inhibited, we treated mice with established tumors with doxy for only 72 hr. We found that at this time point MYC expression is completely inhibited (Figures 1A–1C); however, tumors phenotypically and histologically appear nearly indistinguishable from primary tumors (Figure 1A). At the early stage of tumor regression, we found that there was no substantial change in apoptosis; however, proliferation, as measured by Ki-67 staining, was significantly diminished (Figures 1D–1G). These results indicate that acute inhibition of MYC precedes gross tumor regression.

In addition to following changes in tissue histology, we sought an independent marker of liver tumorigenesis that would allow

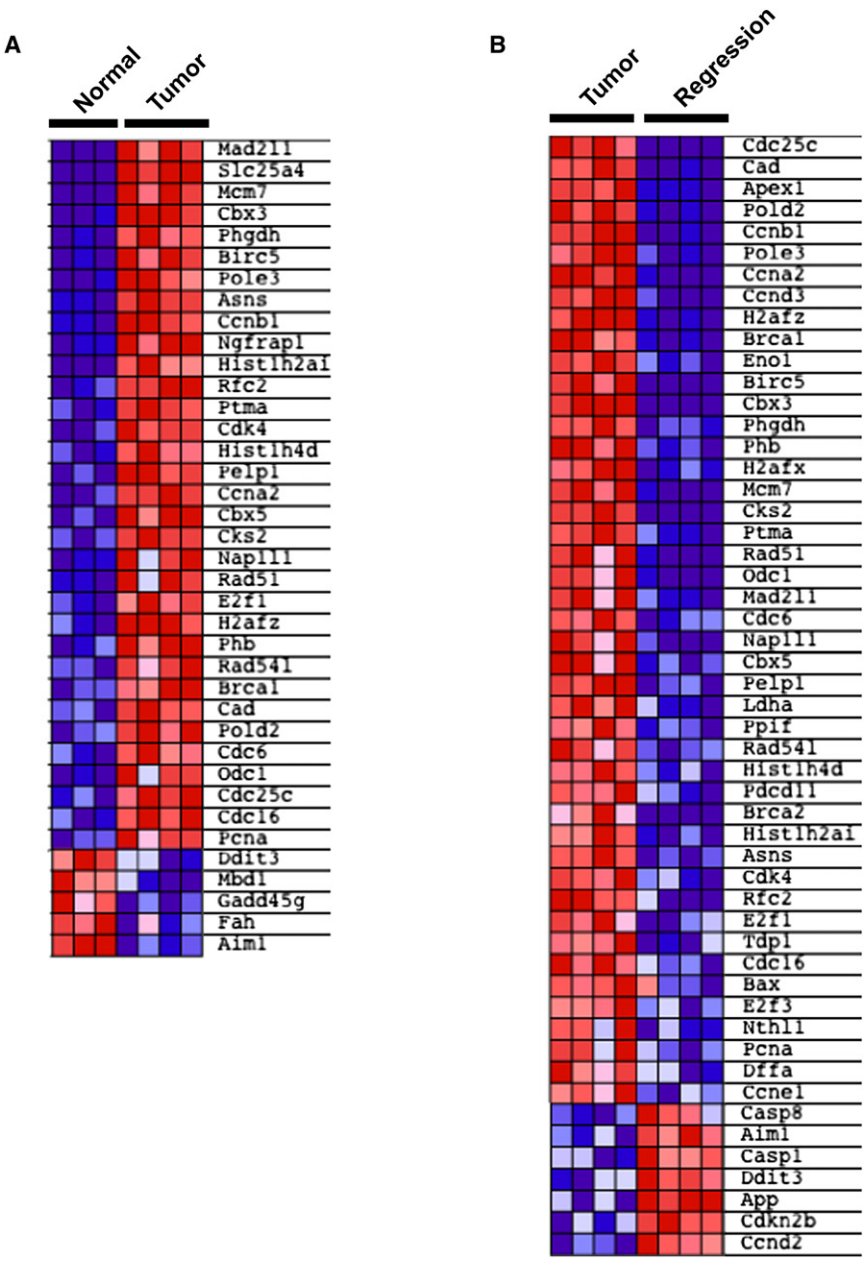

Figure 2. Changes in Gene Expression during *Myc*-Driven Tumor Development and Regression

GSEA analysis of 120 previously reported MYC-regulated genes. Shown are subsets of the 120 genes that are most abundantly enriched or downregulated when comparing normal liver versus tumor tissues (A) or tumor tissues versus early regression samples (B). See also Table S1.

us to examine different liver tumor stages in our models. Alpha-fetoprotein (AFP) is a well-established clinical biomarker of human HCC and hepatoblastoma, but it is not detectable in normal liver. We therefore examined AFP expression in the different stages of liver tumor formation. We found that AFP is not detectable in nontumor LT2 tissues and is negligible in the pretumor LT2/MYC tissues (Figure 1C). In contrast, primary liver tumors demonstrate abundant AFP expression (Figure 1C). After 72 hr of doxy treatment, despite the complete inhibition of MYC expression, there is no discernible decrease in AFP expression (Figures 1B and 1C). Thus, liver tissue histology and AFP expression indicate that MYC expression precedes tumor formation and liver tumor regression follows MYC inhibition.

To better understand the gene expression changes that underlie *Myc*-driven tumor formation and regression, we performed messenger RNA (mRNA) profiling of liver samples at each stage. We selected a subset of 120 genes whose expression is altered in a MYC-dependent manner to determine if gene expression is changed in primary liver tumors as a consequence of inhibiting MYC (Table S1 available online). Most of these genes were previously identified in studies examining gene expression changes in tissue culture models. Genes in this test set are associated with diverse molecular functions including cell cycle, apoptosis, DNA damage, chromatin remodeling, and metabolic pathways such as glycolysis and amino acid metabolic pathways (annotated at http://www.myc-cancer-gene.org/). We performed gene set enrichment analysis (GSEA), a computational method that determines whether there are concordant differences between two groups based on enrichment of the genes in one group compared with the other (Subramanian et al., 2005). This analysis confirmed that MYC target genes were significantly enriched in *Myc* tumors compared to normal livers (Figure 2A, $p < 0.0001$). Likewise, there was an enrichment of the MYC target genes in primary tumors compared to early regression samples (Figure 2B, $p < 0.0001$). Thus, *Myc*-driven tumorigenesis causes widespread changes in gene expression as primary tumors form and as they begin to regress.

Hyperpolarized ^{13}C-Pyruvate Flux into Other Metabolites at Different Stages of *Myc*-Driven Liver Tumor Development and Regression

We next examined whether dynamic changes in metabolic processes occur in vivo and whether any metabolic changes precede overt tumorigenesis using the switchable *Myc* liver tumor model. We evaluated in vivo glycolysis at different stages of liver tumor formation and regression by examining the dynamic flux of pyruvate, a key product of glycolysis, into other metabolites. Hyperpolarized technology utilizing dynamic

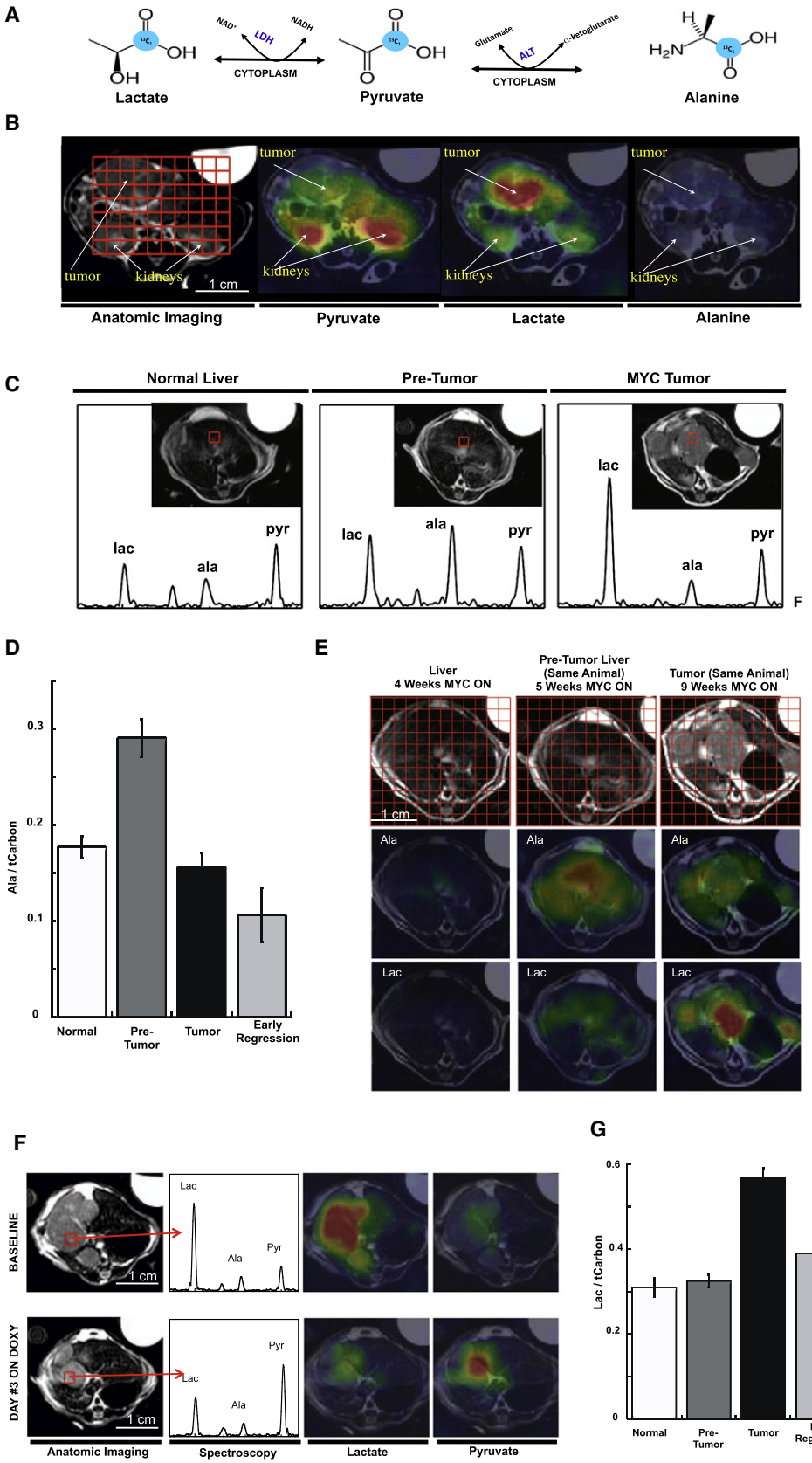
A
Lactate
NAD+
LDH
NADH
CYTOPLASM
Pyruvate
Glutamate
ALT
α-ketoglutarate
CYTOPLASM
Alanine
B
tumor
kidneys
1 cm
Anatomic Imaging
Pyruvate
Lactate
Alanine
C
Normal Liver
Pre-Tumor
MYC Tumor
lac
ala
pyr
F
D
Ala / tCarbon
0.3
0.2
0.1
0
Normal
Pre-Tumor
Tumor
Early Regression
E
Liver
4 Weeks MYC ON
Pre-Tumor Liver
(Same Animal)
5 Weeks MYC ON
Tumor (Same Animal)
9 Weeks MYC ON
1 cm
Ala
Lac
F
BASELINE
DAY #3 ON DOXY
Lac
Ala
Pyr
1 cm
Anatomic Imaging
Spectroscopy
Lactate
Pyruvate
G
Lac / tCarbon
0.6
0.4
0.2
0
Normal
Pre-Tumor
Tumor
Early Regression

nuclear polarization (DNP) (Ardenkjaer-Larsen et al., 2003) can be used with the substrate [1-^{13}C] pyruvate to specifically monitor LDH-catalyzed pyruvate to lactate flux in vivo. Hyperpolarized MRSI overcomes sensitivity limitations in traditional carbon MRSI caused by a low gyromagnetic ratio and low natural abundance of the MR detectable ^{13}C isotope. With a hyperpolarized approach, enhancement of sensitivity on the order of 50,000-fold can be achieved for in vivo metabolic imaging. [1-^{13}C] pyruvate, which is converted to [1-^{13}C] lactate, [1-^{13}C] alanine, and [1-^{13}C] bicarbonate in vivo (Figure 3A), has been recently used to visualize tumor tissues in a lymphoma transplant model as well as in a transgenic prostate cancer model (Albers et al., 2008; Day et al., 2007). In these prior instances, increased pyruvate conversion to lactate was observed in tumor versus adjacent tissue, however, in neither of these prior studies was the temporal association between oncogene signaling, LDH activity and in vivo glycolysis examined.

In the cell, pyruvate may be converted to acetyl co-A, lactate or via transamination, into alanine. Conversion of pyruvate into lactate or alanine (Figure 3A) can be visualized by MRSI. We first examined the flux of pyruvate into other metabolites in established LT2/MYC liver tumors. MR anatomic imaging was used to visualize liver tumors, nontumor tissues, and adjacent normal structures. Applying a compressed sensing technique, which allows rapid image acquisition across an entire liver, we performed hyperpolarized ^{13}C 3D spectroscopic imaging with 0.034 cm^3 per voxel resolution (Hu et al., 2010). Using this approach, metabolic imaging of an entire mouse was achieved in ~16 s (Figure 3B). We found that ^{13}C-pyruvate could be readily detected in nontumor tissues such as the kidneys (Figure 3B). In contrast, ^{13}C-lactate was abundantly detected only in tumor and not in adjacent tissues (Figure 3B). ^{13}C-alanine was not appreciably detected in established tumors (Figure 3B). Thus, consistent with prior studies, tumor tissues have increased flux of pyruvate to lactate consistent with increased LDH activity.

We next asked whether ^{13}C-pyruvate flux changes during the course of primary liver tumor development. We imaged normal liver, pretumor liver tissues, and established tumors using ^{13}C-pyruvate 3D spectroscopic imaging (Figure 3C). We found that in pretumor tissues there is a significant increase in the conversion of ^{13}C-pyruvate to ^{13}C-alanine, which was not present in either nontumor tissues or established tumors (Figures 3C and 3D). Thus, conversion to alanine is the earliest metabolic change we detected and this preceded primary tumor formation. A sampling of spectra from various liver regions over the course of disease progression shows that while the average alanine signal is increased in the pretumor state, there is considerable heterogeneity between individual voxels in the pretumor liver (Figure 3E). We found that the regions in pretumor tissue with the most abundant alanine signal tended to be areas where tumor nodules would eventually develop. Thus, using this approach we can detect specific areas with elevated alanine levels in the pretumor state compared to the rest of the liver.

We next asked how ^{13}C-pyruvate flux is altered when MYC is inhibited in established tumors. We imaged tumors at baseline and then again 3 days after the mice were fed a diet containing doxy to switch off MYC expression (Figures 1A–1C). After 3 days of doxy treatment, liver tumors began to diminish in size, although substantial tumor mass was still present (Figure 3F) and was histologically indistinguishable from untreated tumors (Figure 1A). We examined ^{13}C-pyruvate flux in the tumor tissue after MYC inhibition. We found a dramatic reversal of the ^{13}C-pyruvate flux to lactate in early tumor regression (Figure 3F). Thus, the ratio of ^{13}C-lactate to total carbon rapidly returns to levels present in nontumor tissue after MYC inhibition (Figure 3G).

In a series of control experiments, we found that constitutive expression of the tTA transcription factor in hepatocytes of LT2 transgenic mice compared to wild-type mice did not affect Lac/tCar or Ala/tCar ratios (Figure S1A). Likewise, doxy treatment of nontumor bearing mice did not alter in vivo metabolic flux to either alanine or lactate (Figure S1B). This indicates that the results are not due to underlying toxicity from doxy treatment or transgene expression. We therefore conclude that inhibiting MYC in an established liver tumor inhibits glycolysis, resulting in diminished pyruvate to lactate flux.

We sought to understand the molecular basis for differences in ^{13}C-pyruvate flux in livers at different stages of *Myc*-driven tumorigenesis. We first examined changes in gene expression of molecules that may impact ^{13}C-pyruvate flux. The MCT1 transporter (SLC16A1) has been proposed to alter uptake of pyruvate into cells (Harris et al., 2009). We did not detect appreciable differences in MCT1 expression in tumor tissues or upon early tumor regression (Figure S1C). Moreover, the imaging studies were normalized to total ^{13}C signal (tCar) and

Figure 3. Hyperpolarized ^{13}C Metabolic Imaging of Liver Tumor Formation and Regression

(A) Diagram showing the conversion of ^{13}C-pyruvate to lactate or alanine.

(B) Color overlay maps from spectroscopic grids show clear differences in metabolic profiles between liver tumors and other tissues.

(C) Hyperpolarized imaging reveals changes in metabolic profile during *Myc*-driven tumor formation. High pyruvate is detected in normal liver. Elevated alanine is associated with pretumor liver with modest MYC induction but no apparent phenotypic changes. A substantial increase in lactate is seen in developed tumor masses.

(D) A significant and reproducible pattern of high alanine in pretumor liver compared to controls ($p = 0.003$) and tumor ($p = 0.0002$) is observed.

(E) Heterogeneous elevation of alanine may correspond to areas of eventual tumor development. Color overlays generated from spectral grids are shown for a single animal over the course of disease progression after oncogene activation. The first column shows a healthy liver that has uniformly low alanine and lactate levels. The middle column shows a change in metabolic profile one week later, with substantially elevated alanine signal now observed. The alanine overlay highlights heterogeneity in the liver (bright red regions corresponding to highest signal intensity). The final column shows the liver 9 weeks after *Myc* activation, now consisting of a heterogeneous collection of distinct tumor nodules and regions of nontumor. The lactate overlay shows the tumor nodules as the regions with the highest lactate signal intensity. Color intensities were normalized across the different time points according to metabolite.

(F) Imaging early tumor regression before and 72 hr after MYC inhibition. A dramatic decrease in lactate is detected in voxels at similar locations prior and after doxy treatment. Spectra for the indicated voxel and corresponding anatomic imaging are shown.

(G) Repeated studies demonstrated a significant increase in lactate during tumor formation compared to controls ($p < 0.0001$) and decrease upon early regression ($p < 0.0002$). Lactate and alanine are reported as normalized to total carbon (the sum of lactate, alanine, and pyruvate).

Error bars represent the SEM. See also Figure S1.

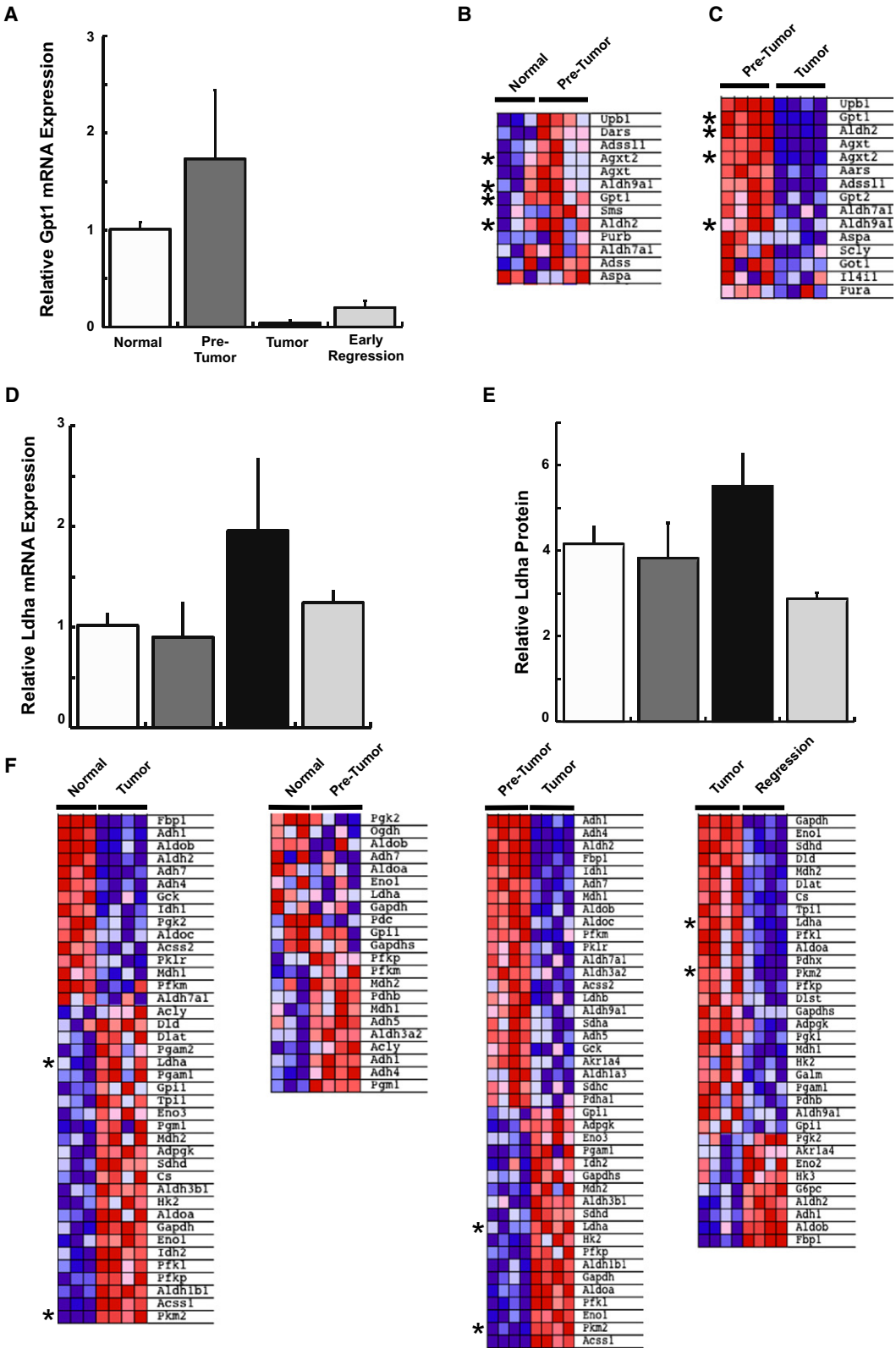

Figure 4. Expression of Key Regulators of the Alanine and Glycolysis Biosynthetic Pathways Is Altered at Different Stages of *Myc*-Driven Liver Tumor Development

(A) Gpt1 mRNA expression significantly increases during early-stage pretumors and decreases in fully developed liver tumors.

changes in MCT1 expression could be accounted for with this normalization.

Increased Alanine Metabolism Precedes Tumor Formation

We next examined gene expression changes in enzymes that regulate alanine and lactate production. The GPT1 (ALT) transaminase is a central regulator of pyruvate to alanine conversion. We found that GPT1 expression was moderately increased in pretumor tissues, consistent with the increased ^{13}C-alanine observed in pretumor tissues (Figure 4A). In contrast, in tumor tissues or early regression samples GPT1 expression was dramatically decreased (Figure 4A). This is consistent with the absence of appreciable Ala / tCar found in imaging studies of established tumors.

We next asked whether in addition to *Gpt1* other genes in the alanine biosynthetic pathway are also upregulated in pretumor tissues. Increased alanine production has been observed in association with cancer-related cachexia (Heber et al., 1985). Alanine can also be used for gluconeogenesis, generate cellular ATP, alter cellular redox potential and generate macromolecule intermediates useful for anabolism (Berg et al., 2002; Schindhelm et al., 2006), but to our knowledge this pathway has not been previously investigated as an early marker of tumor formation. Using the KEGG pathway database (http://www.genome.jp/kegg/), we examined 20 genes associated with alanine metabolism and found that most are upregulated in early-stage samples compared to normal livers (Figure 4B and Table S2, $p < 0.004$). In contrast, most of the alanine-pathway genes are downregulated in the primary tumors compared to pretumor samples and remained low upon tumor regression (Figure 4C and Table S2, $p < 0.005$). Thus, increased expression of genes associated with alanine metabolism was associated with precancerous, early stages of tumor formation, but not in normal controls or primary and regressing tumors. Besides lactate, alanine is a major source of cytosolic pyruvate and transamination enables interconversion of alanine and pyruvate, which may then be used for gluconeogenesis or anabolic processes. Thus, our mRNA expression analysis shows that changes in genes associated with alanine metabolism precede primary tumor formation and raise the possibility that specific metabolic markers, such as alanine, may be useful to identify the earliest stages of tumor formation.

We next examined metabolic changes associated with primary tumors and early regression. *Ldha* has been shown to be the major mediator of tumor-associated glycolysis across various tumor types (Fantin et al., 2006; Vander Heiden et al., 2009) by converting pyruvate to lactate. The *Ldha* gene is also a direct transcriptional target of *Myc* in lymphoma and engineered fibroblast cells (Shim et al., 1997). We found that LDHA expression is similar in normal liver and pretumor tissues with low MYC expression (Figure 4D). In primary tumors, LDHA expression was increased substantially compared to normal liver, but expression returned to normal once MYC expression was inhibited in the early regression tumor samples (Figure 4D). Quantitative western blotting for LDHA also revealed similar results (Figure 4E).

While *Ldha* is a key regulator of glycolysis in tumor tissues (Dang and Semenza, 1999; Le et al., 2010), we asked whether multiple glycolytic enzymes are coordinately upregulated in primary tumors. We determined the expression of 72 genes associated with glycolysis (http://www.genome.jp/kegg/) and found that many glycolytic pathway genes, including *Ldha* and another key regulator, *Pkm2* (Christofk et al., 2008; Vander Heiden et al., 2009), were enriched in tumor samples compared to normal liver and pretumor samples (Figure 4F and Table S2). In contrast, once *Myc* was switched off, diminished expression of multiple glycolytic genes including *Ldha* and *Pkm2* (Figure 4F and Table S2, $p < 0.007$) was found in early regression samples. Thus, many, although not all, genes associated with the glycolysis-pathway are dynamically regulated as a consequence of *Myc* oncogene signaling as primary tumors form and regress.

Increased ALT and LDH Enzyme Activities Correlate with the Corresponding Metabolic Imaging Biomarkers

While the changes in *Gpt1* and *Ldha* mRNA abundance observed in liver tumor formation and regression are consistent with the observed changes in metabolic imaging, additional translational or posttranslational modifications could potentially also alter enzymatic activity that could not be accounted for entirely by differences in mRNA abundance. We therefore thought it was critical to determine the enzymatic activity of these molecules in liver tissues at different stages of tumorigenesis. To directly link changes of ^{13}C-pyruvate flux observed during in vivo imaging to enzyme activity, we collected liver tissues immediately after imaging. Animals were sacrificed and tissues were collected for enzymatic activity assays. We found significantly elevated ALT enzyme activity in pretumor tissues compared to normal tissues or primary tumors and a correlation between ALT activity and Alanine/tCar ratio (Figure 5A, $R = 0.47$, $p = 0.05$). Finally, we also found a strong correlation between LDH Vmax and Lactate / tCar imaging (Figure 5B, $R = 0.76$, $p < 0.0005$).

Expression of Glutamine and Tricarboxylic Acid Cycle Pathway Genes Changes as Tumors Form and Regress

Several prior studies have identified increased glutamine uptake and catabolism as an important energy source in cells that overexpress MYC (Dang, 2010; Wise et al., 2008; Yuneva et al., 2007), but the in vivo importance of this pathway is less clear. While our current studies with ^{13}C-pyruvate imaging do not allow us to directly visualize glutamine catabolism, this pathway can

(B) GSEA analysis of alanine-pathway genes reveals upregulation of many genes in the pathway in pretumor samples compared to normal liver ($p < 0.004$). Enriched genes are shown.

(C) GSEA analysis of alanine-pathway genes comparing pretumor and tumor samples shows downregulation of genes in this pathway ($p < 0.005$). Genes enriched in pretumors are shown. Alanine-pathway genes described in the text are indicated with an asterisk.

(D and E) *Ldha* mRNA (D) and protein expression (E) show elevated *Ldha* expression only in primary tumors.

(F) GSEA analysis of glycolysis genes showing two-way comparisons of glycolytic pathway gene expression at different states of tumor formation and regression. Key glycolysis regulators *Ldha* and *Pkm2* are indicated with an asterisk.

Error bars represent the SEM. See also Figure S2 and Table S2.

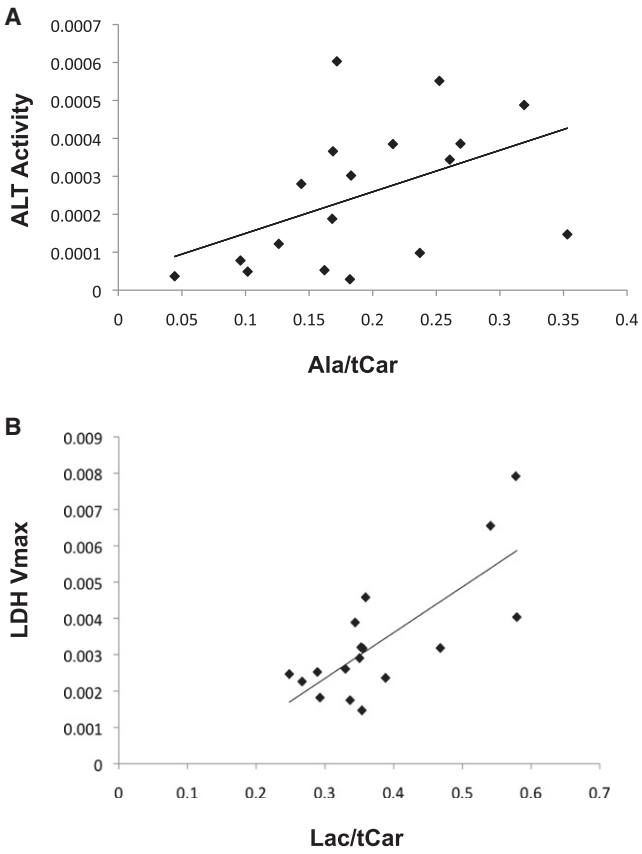

Figure 5. ALT and LDH Enzyme Activities Correlate with the Corresponding Metabolic Imaging Biomarkers

(A) Graph of ALT activity versus alanine/tCar levels across various treatment conditions demonstrates a correlation between imaging and enzyme activity ($p = 0.05$).

(B) Graph of LDH activity versus lactate/tCar levels across various treatment conditions demonstrates a correlation between imaging and enzyme activity ($p < 0.0005$).

feed into alanine production. We therefore examined whether the expression of glutamine-pathway genes (Table S3) is altered in primary liver tissues as tumors form and regress. We find that a number of genes in this pathway are increased in the transition from normal to the pretumor state including glutamate dehydrogenase (*Glud1*) and the mitochondrial form of glutamic-oxaloacetic transaminase (*Got2*) (Figure 6A). The glutaminase genes (*Gls* and *Gls2*) were upregulated in only a subset of the pretumor tissues (Figure 6A). Two glutamine transporters, *Slc5a1* and *Slc7a1*, are direct transcriptional targets of *Myc* (Dang, 2010). We found that *Slc7a1* was modestly upregulated in a subset of pretumor specimens compared to normal liver. With progression from the pretumor to tumor state we find that *Slc7a1*, *Got2*, and *Gls* are substantially further upregulated, while *Glud1* and *Gls2* are markedly downregulated (Figure 6A). Finally, there is a rapid reversal of these gene expression changes as tumors begin to regress, with *Glud1* and *Gls2* increasing and *Slc7a1*, *Gls*, and *Got2* being rapidly suppressed (Figure 6A). Our results demonstrate that gene expression of the glutamine pathway genes are altered during different stages of tumor formation, and are consistent with increased glutamine catabolism in *Myc*-driven liver tumors and rapid shutoff as tumors begin to regress.

The *Myc* oncogene in addition to promoting glycolysis has also been shown to increase mitochondrial biogenesis (Kim et al., 2008; Li et al., 2005). Thus it has been proposed that *Myc* may provide dual functions by driving both aerobic glycolysis and oxidative phosphorylation when sufficient oxygen is present (Dang, 2010). In addition to being converted to alanine or lactate, pyruvate can also be converted to CO_2 and acetyl-CoA, which can enter the mitochondrial TCA cycle. [1-^{13}C]-pyruvate MRSI does not allow us to readily visualize the pyruvate that is converted to CO_2 with high sensitivity. We therefore examined the gene expression changes of key regulators of the TCA cycle (Figure 6B and Table S3). Pyruvate dehydrogenase (*Pdha1*), the key regulator of pyruvate entry into the TCA cycle was elevated in the majority of pretumor tissues, but decreased as they progressed to tumors (Figure 6B). This is consistent with an increase in glycolysis in tumor tissues. Interestingly, however, *Pdha1* was further downregulated in the early regression samples compared to primary tumors. Thus, the inability of *Pdha1* to be upregulated as tumors regress, may explain, at least in part, the rapid exit of tumor cells from the cell cycle (Figures 1D and 1F) if sufficient energy production cannot be sustained via the TCA cycle and subsequent oxidative phosphorylation. We also examined the expression of Pyruvate dehydrogenase kinase enzymes responsible for inactivating the Pyruvate dehydrogenase complex and preventing glucose breakdown. The different isoenzymes (*Pdk1–Pdk4*) showed deregulated patterns of expression in each of the stages analyzed (Figure 6B).

DISCUSSION

Increased conversion of glucose into lactate has been observed in tumor cells in culture; however, the ability to visualize dynamic changes in glycolysis as a function of oncogene signaling in vivo has been previously lacking. In this study, we sought to identify different stages of liver tumor formation and regression when the driving oncogene c-*Myc* was temporally regulated. We used hyperpolarized technology to assess metabolic consequences of *Myc*-driven liver tumor progression and regression. We found a strong correlation between LDH activity and in vivo conversion of pyruvate to lactate. Multiple glycolysis-pathway genes are upregulated in tumors, and their expression is rapidly repressed when *Myc* is switched off (Figures 4 and 7). This MR-based system enables both rapid metabolic assessments and anatomical imaging. Use of hyperpolarized ^{13}C-pyruvate MRSI allows for noninvasive visualization of glycolytic changes within a de novo tumor beyond uptake and the first enzymatic step.

Interestingly, we found that metabolic changes precede both tumor formation and regression. The earliest metabolic change observed was increased alanine in heterogeneous regions of the pretumor livers. *Gpt1* gene expression and ALT enzymatic activity were elevated in this pretumor state and corresponded to the elevated Ala/tCar observed (Figure 7). Whether the elevated Ala/tCar spectra found is unique to livers in which *Myc* is the driving oncogene remains unknown. However, many MYC target genes potentially connect to increased alanine production. Multiple genes in the glutamine metabolic pathway

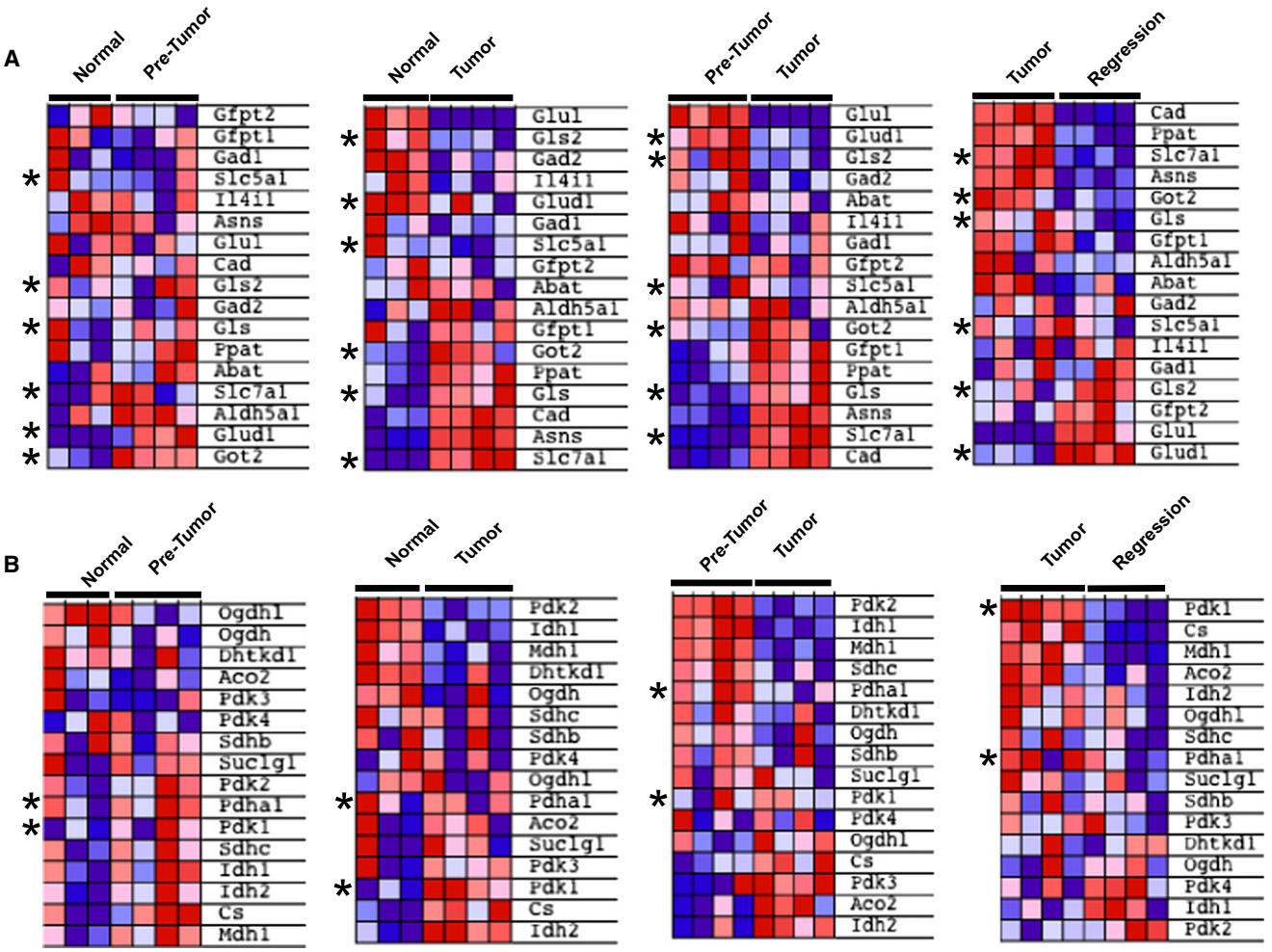

Figure 6. Expression of Glutamine and TCA Cycle Pathway Genes as Tumors Form and Regress

(A) GSEA analyses of a subset of glutamine metabolism genes show an increase in expression as tumors develop and decrease in expression as they regress. Key regulators discussed in the text are indicated with an asterisk.

(B) GSEA analysis of TCA cycle genes. Key regulators *Pdha1* and *Pdk1* are indicated with an asterisk.

See also Table S3.

are regulated by MYC signaling, including glutaminase (*Gls*) and the glutamine transporters (*Slc5a1* and *Slc7a1*). GLS acts to convert glutamine to glutamate. Increased glutamate, along with pyruvate, is then converted by ALT to alanine and α-ketoglutarate, which in turn may enter the TCA cycle. Thus, elevated alanine production may be, in part, due to increased glutamine uptake and catabolism in pretumor tissues to glutamate (Figure S2).

We also examined other alanine pathway genes whose expression was altered in the pretumor state and found that two genes, *Aldh2* and *Aldh9a1*, are known to be direct MYC targets (http://www.myc-cancer-gene.org/). Both genes are also substantially upregulated in pretumor tissues compared to tumors (Figure 4B and Figure S2). Both *Aldh2* and *Aldh9a1* can participate in the production of beta-alanine from polyamine degradation. Beta-alanine plus pyruvate can in turn be converted into L-alanine and 3-oxopropanoate by alanine-glyoxylate aminotransferase 2 (*Agxt2*). *Agxt2* is upregulated in the pretumor state compared to normal liver and is diminished in primary tumors (Figures 4B and 4C). Ornithine decarboxylase (*Odc1*), a canonical MYC target gene, is rate limiting for polyamine synthesis and is upregulated in both pretumor cells and tumors. Thus, it is possible that MYC may regulate alanine production at the pretumor state both by upregulating polyamine synthesis (via direct regulation of *Odc1*) and by their conversion into beta-alanine (via direct regulation of *Aldh2* and *Aldh9a1* in pretumor tissues). Why *Odc1* expression remains high in tumors, while *Aldh2* and *Aldh9a1* expression diminishes is unclear, but it is well established that MYC may function as both a transcriptional activator and repressor depending on specific cellular contexts. Thus, there may be multiple *Myc*-driven pathways leading to increased alanine production in the pretumor state. However, it remains to be determined whether other oncogenes can also upregulate the alanine pathway in pretumor tissues. As imaging and hyperpolarization techniques continue to improve, it should be possible to discern with increasing resolution if the

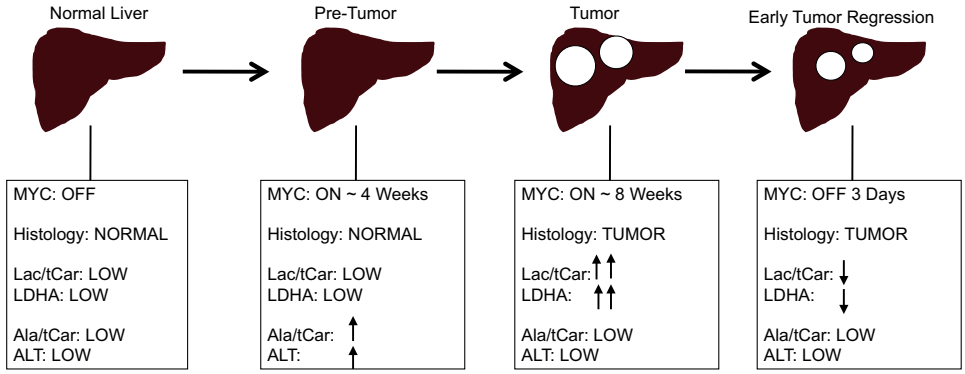

Figure 7. Changes in Metabolism Correlate with Stages of *Myc*-Driven Liver Tumor Development and Regression
Schema summarizing the Lactate/tot Carbon, LDHA Vmax, Alanine/tot Carbon, ALT activity levels, and metabolic gene expression changes in the different stages of *Myc*-induced liver tumor progression and regression.

pretumor tissues with the highest alanine production will ultimately develop into liver tumor nodules.

Finally, in the present study we employed a transgenic liver tumor model driven by the *Myc* oncogene. Other oncogenes, including activated alleles of *Ras*, *Akt*, and *Pik3ca*, or loss of tumor suppressors (such as *p53* and *Vhl*) have also been shown to increase glycolysis (Dang, 2009). Thus, the deregulation of many glycolytic genes is not necessarily directly regulated by MYC or unique to *Myc*-driven tumors. Therefore, this approach should have utility beyond tumors driven by the *Myc* oncogene. Metabolic imaging via ^{13}C-pyruvate is a rapid, nonradioactive approach to visualize glycolysis and alanine pathway changes in vivo and should provide new metabolic markers of cancer progression and regression. Clinical studies employing ^{13}C-pyruvate MRSI imaging technology to visualize tumors in patients have recently begun. We propose that this approach may have utility to identify metabolic changes at the earliest steps of tumor formation and regression.

EXPERIMENTAL PROCEDURES

Mouse Tumor Model

Tet-o-MYC/LAP-tTA (LT2/MYC) double-transgenic mice were obtained by crossing two transgenic FVB strains (Goga et al., 2007). Under this system, the Tet transactivator drove MYC expression only in the liver. MYC expression could be inactivated by doxy to bind and inactivate the Tet transactivator. The Tet-o-MYC/LAP-tTA mice were weaned on doxy (200 mg/kg) until 4 weeks of age. Doxy was then removed from the diet to allow induction of expression of the human c-*Myc* transgene and tumorigenesis. Mice were monitored weekly for tumor development by inspection and palpating the abdomen. Tumors were confirmed by MR anatomic imaging. All animal studies were carried out under a protocol approved by the University of California, San Francisco (UCSF) Institutional Animal Care and Use Committee.

Liver Histology and staining

Tissue sections from normal livers of control (LT2) mice, pretumor liver tissue and primary tumors from established or regressing LT2/MYC tumors were stained using a standard hematoxylin and eosin (H&E) protocol. Tumor morphology and tissue histology were examined. c-MYC (Epitomics, 1492) antibody was used to stain liver tissue sections for MYC. Ready-to-use Ki67 antibody (NeoMarkers) was used for Ki67 staining. TUNEL was performed with the ApopTag Peroxidase In Situ Apoptosis Detection Kit (Millipore). All staining was performed on formalin-fixed, paraffin embedded, 5 μm tissue sections of mouse livers.

Real-Time Quantitative PCR

Gene expression was determined by real-time quantitative PCR. Liver tissues from four representative samples from each group, normal LT2, early-stage pretumors, established primary tumors, and regressing tumors were analyzed. Total RNA from liver tissues was extracted (mirVana mirna isolation kit, Ambion), followed by Dnase treatment (Turbo DNA-free Dnase Treatment kit, Ambion) according to the manufacturer's protocol. Complementary DNA (cDNA) from 1 μg DNase-treated total RNA was synthesized with the iScript cDNA synthesis Kit (Bio-Rad). Real-time PCR was carried out with TaqMan probes (Applied Biosystems) for MYC, LDHA, and GPT1 and SYBR green (Applied Biosystems) for MCT1 and compared to expression of the housekeeping gene, GAPDH.

Western Blot Analysis

Antibodies for c-MYC (Epitomics, 1492), AFP (NeoMarkers, RB-365-A1), and ACTIN (Sigma, A-1978) were purchased and used as indicated by the respective manufacturers.

mRNA Microarrays

Total RNA from LT2 controls (n = 3), pretumor early-stage samples (n = 4), established LT2/MYC liver tumors (n = 4), and early regression tumor samples (n = 4) was extracted (mirVana mirna isolation kit, Ambion). RNA quality was assessed with the Nanodrop ND-8000 (Nanodrop Technologies) and a Pico Chip on an Agilent 2100 Bioanalyzer (Agilent Technologies) and run on Agilent mouse whole genome 4x44K Ink-jet arrays. Sample preparation, labeling, and array hybridizations were performed according to standard protocols from UCSF Shared Microarray Core Facilities and Agilent Technologies (http://www.arrays.ucsf.edu/ and http://www.agilent.com/). RNA was amplified with the Sigma whole transcriptome amplification kit (Sigma-Aldrich), and subsequent Cy3-CTP labeling was performed with NimbleGen one-color labeling kits (Roche-NimbleGen). The labeled DNA was assessed with Nanodrop 8000, and equal amounts of Cy3 labeled target were hybridized to Agilent mouse whole genome 4x44K Ink-jet arrays. Hybridizations were performed for 14 hr, according to the manufacturer's protocol (Agilent). Arrays were scanned with the Agilent microarray scanner, and raw signal intensities were extracted with Feature Extraction v10.1 software.

Primary normalization and data extraction were done by the Microarray Core Facility. In brief, raw log-intensities were normalized via the quantile normalization method (Bolstad et al., 2003). No background subtraction was performed, and the median feature pixel intensity was used as the raw signal before normalization. A one-way ANOVA model was used and specific contrasts were formulated to examine pair-wise comparisons of interest.

Microarray Data Analyses

Effect of Inactivation of the Myc *Oncogene in Liver Tumor Models*

Subsets of MYC target genes belonging to different pathways frequently reported to be targeted by MYC were selected from the MYC cancer gene

database (http://www.myc-cancer-gene.org/ and Table S1). Genes selected are associated with various pathways, including cell cycle, apoptosis, DNA repair, chromatin remodeling, and glycolysis, alanine, and glutamine metabolic pathways. Hierarchical clustering was performed, and the four study groups (LT2 controls, pretumor early-stage mice, established LT2/MYC liver tumor, and regressing LT2/MYC liver tumor mice) were compared.

Comparison of Specific Metabolic Pathways in Developing and Regressing Myc-Driven Liver Tumors

Expression of genes associated with energy and anabolic metabolic pathways such as glycolysis and alanine metabolism was compared in the four study groups via GSEA (Subramanian et al., 2005). Gene lists for the glycolysis and alanine metabolic pathways were obtained from the KEGG database (http://www.genome.jp/kegg/pathway.html).

GSEA was used to determine the significance of differentially expressed MYC target genes and specific metabolic pathways in normal livers, early-stage pretumors, primary developed tumors, and tumors in early regression. Predefined gene lists including 120 MYC targets genes from multiple pathways regulated by MYC, 78 glycolysis genes, and 20 alanine metabolism genes were used in GSEA. The gene set permutation was used instead of phenotype in order to avoid the potential problem of a small sample size.

Dynamic Nuclear Polarization and Injection of Hyperpolarized Pyruvate

The dynamic nuclear polarization and data acquisition protocols are described previously (Hu et al., 2010). An aliquot of 24 μl [1-^{13}C] pyruvic acid with 15 mM OX63 trityl radical and 1.5 mM Dotarem gadolinium were polarized for 1 hr in a 3.35T magnetic field at 1.35 Kelvin with a Hypersense DNP polarizer (Oxford Instruments, Abingdon, UK). The power of the microwave irradiation was 20 mW. The solvent used to dissolve the frozen solid state sample was an aqueous mixture containing 40 mM Tris, 80 mM NaOH, and 0.3 mM Na_2EDTA. The resulting pyruvate concentration was 80 mM, with a pH of ~7.5 and polarizations greater than 30% upon dissolution. A 350 μl volume of the dissolved pyruvate, followed by a 150 μl saline flush, was injected into mice through a tail vein catheter. A compressed sensing pulse sequence with 0.034 cm^3 voxel resolution was used to acquire 3D MRSI data. The uptake of ^{13}C-pyruvate and conversion to ^{13}C-lactate and ^{13}C-alanine were monitored with 3D spectroscopic imaging as described below. Mice were anesthetized with isoflurane and kept warm with a circulating-water heating pad.

Magnetic Resonance Imaging and Spectroscopic Imaging

All experiments were performed on a General Electric 3T (Waukesha, WI) MRI scanner equipped with 40 mT/m, 150 mT/m/ms gradients, and a broadband RF amplifier. The RF coil was a custom built, dual-tuned ^{1}H/^{13}C transmit/receive design used previously (Albers et al., 2008; Hu et al., 2010). T2-weighted proton fast spin-echo (FSE) images were acquired and used as the anatomical reference on which ^{13}C spectra were overlaid and coregistered. The axial FSE imaging parameters were as follows: FOV = 8 cm, 192 × 192 matrix, 2 mm slice thickness, and NEX = 6. Carbon-13 hyperpolarized spectra were acquired as a volumetric grid with a compressed sensing 3D-MRSI sequence (Hu et al., 2010). Acquisition parameters were as follows: variable flip angle, TE = 140 ms, TR = 215 ms, 16 × 16 in-plane phase encodes, center out phase encode order, 2.5 mm × 2.5 mm in-plane resolution, flyback readout in z with 16 points and 5.4 mm resolution, 581 Hz spectral bandwidth, and 9.8 Hz spectral resolution. The ^{13}C 3D-MRSI scan was started 30 s after injection of the hyperpolarized ^{13}C-pyruvate and lasted 16 s. To quantify metabolism in the ^{13}C spectra, the areas under the ^{13}C-lactate, ^{13}C-pyruvate-hydrate, ^{13}C-alanine, and ^{13}C-pyruvate peaks (total carbon-13 defined as the sum of all four) in magnitude spectra were calculated. The ratios lactate area to total carbon area (Lactate/tCar) and alanine area to total carbon (Alanine/tCar) were computed for each voxel and then averaged over all voxels of interest for each mouse to derive the final lac/tCar and ala/tCar values for statistical analysis.

Ex Vivo LDH Activity

Total LDH activity was measured through an NADH-linked spectrophotometric method by observing the decrease in absorbance of NADH at 339 nm after addition of varying concentrations of pyruvate. Around 0.2 g of frozen tissue was thawed in lysis buffer containing 50 mM Tris (pH 8.2), 2 mM DTT, 2 mM EDTA, and 1% Triton x-100. The tissue was homogenized and centrifuged for 1 min at 7000 rpm at 4°C. The supernatant was removed and diluted appropriately so that the reduction of NADH was linear over the first ten minutes of the assay. In microplate wells, 3 μl cell lysate was mixed with 147 μl reaction buffer containing varying concentrations of pyruvate, 80 mM Tris (pH 7.2), 200 mM NaCl, and 200 μM NADH that was heated to 30°C. The assay was conducted immediately by monitoring the decrease in NADH absorbance, at 339 nm, for 10 min with an Infinite M200 spectrophotometer (Tecan). Each pyruvate concentration was assayed in triplicate. The reaction rate was normalized to total protein concentration (Quick Start Bradford Protein Assay, Bio-Rad). Each sample was assayed in triplicates, at 595 nm, after incubating at room temperature for at least 5 min. The absorbance of the sample was then recorded, and protein concentration calculated with a gamma-globulin standard curve. Once the sample's protein concentration had been acquired, it was used to calculate LDH reaction rate for the varying pyruvate concentrations. The LDH reaction rate, measured in μM NADH/min/[protein], was plotted against pyruvate concentrations according to Michaelis-Menten kinetics. The maximum velocity (Vmax) and Km values were then calculated with the Lineweaver-Burk plot.

Ex Vivo ALT Activity

ALT activity was measured with a commercially available enzymatic assay kit (MaxDiscovery). A coupled reaction scheme was used in which the first step was alanine and alpha-ketoglutarate conversion to glutamate and pyruvate by ALT. Pyruvate and NADH were then converted to lactate and NAD+ by lactate dehydrogenase, and activity was detected spectrophotometrically by measurement of absorbance at 339 nm.

Statistical Analysis

All statistical analysis was performed with the JMP software package. For the ^{13}C MRSI statistical analysis, experimental data were divided into four groups: normal liver (Tet transactivator control mice [n = 5]), pretumor (Tet-o-MYC/LAP-tTA mice with *Myc* on >30 days and no tumor on anatomic imaging [n = 5]), tumor (Tet-o-MYC/LAP-tTA mice with *Myc* on and tumor confirmed by anatomic imaging [n = 8]), and early regression (Tet-o-MYC/LAP-tTA tumor mice in which *Myc* has been off for 72 hr [n = 4]). For animals with repeat acquisitions, e.g., two scans in a row to determine reproducibility, the average of the measurements was used. Normal liver, pretumor, tumor, and early regression groups were compared with Tukey's test after a one-way ANOVA was performed. Note that four mice in the Tumor group had a baseline ^{13}C MRSI imaging exam and a repeat 72 hr after MYC was kept on. The four mice in the early regression group received a ^{13}C MRSI baseline study and then a follow-up 72 hr after inhibiting MYC. Thus, there are eight total animals in the tumor group (in which a baseline tumor ^{13}C MRSI was performed) and four in the early regression group. Consequently, tissues were collected from four tumor group mice and four early regression group mice. For the expression comparisons, a Student's t test was used, and for enzyme activity correlations, the Pearson product-moment was computed, after which the Student's t test was used to test for statistical significance.

ACCESSION NUMBERS

Microarray data are available from the Gene Expression Omnibus under accession number GSE28198.

SUPPLEMENTAL INFORMATION

Supplemental Information includes two figures and three tables and can be found with this article online at doi:10.1016/j.cmet.2011.04.012.

ACKNOWLEDGMENTS

We thank Noelle L'Etoile and members of the Goga and Vigneron labs for helpful discussions. We thank Mercedes Joaquin for mouse colony care and genotyping, Kristen Scott for her assistance in the animal imaging studies, and Paniz Vafaei for her work on the LDH and ALT activity assays. We thank David Erle, Andrea Barczak, Yuanyuan Xiao, and Rebecca Barbeau from the

Sandler Asthma Basic Research (SABRE) Center Functional Genomics Core Facility and NIH/NCCR UCSF-CTSI grant number UL1RR024131. We thank Linda Prentis for help with processing liver tissue samples. This work was supported by NIH R21CA137298 (to D.V. and A.G.), K08CA104032 and 1R01CA136717 (to A.G.), R01EB007588 and P41EB013598 (to D.V), UCSF Liver Center grant P30DK026743, and GE Healthcare. A.G. is a V-Foundation Scholar. The funders had no role in study design, data collection and analysis, decision to publish, or preparation of the manuscript.

Received: November 19, 2010
Revised: February 19, 2011
Accepted: April 4, 2011
Published: July 5, 2011

REFERENCES

Albers, M.J., Bok, R., Chen, A.P., Cunningham, C.H., Zierhut, M.L., Zhang, V.Y., Kohler, S.J., Tropp, J., Hurd, R.E., Yen, Y.F., et al. (2008). Hyperpolarized 13C lactate, pyruvate, and alanine: noninvasive biomarkers for prostate cancer detection and grading. Cancer Res. *68*, 8607–8615.

Ardenkjaer-Larsen, J.H., Fridlund, B., Gram, A., Hansson, G., Hansson, L., Lerche, M.H., Servin, R., Thaning, M., and Golman, K. (2003). Increase in signal-to-noise ratio of > 10,000 times in liquid-state NMR. Proc. Natl. Acad. Sci. USA *100*, 10158–10163.

Berg, J.M., Tymoczko, J.L., Stryer, L., and Stryer, L. (2002). Biochemistry (New York: W.H. Freeman).

Bolstad, B.M., Irizarry, R.A., Astrand, M., and Speed, T.P. (2003). A comparison of normalization methods for high density oligonucleotide array data based on variance and bias. Bioinformatics *19*, 185–193.

Cairo, S., Armengol, C., De Reyniès, A., Wei, Y., Thomas, E., Renard, C.A., Goga, A., Balakrishnan, A., Semeraro, M., Gresh, L., et al. (2008). Hepatic stem-like phenotype and interplay of Wnt/beta-catenin and Myc signaling in aggressive childhood liver cancer. Cancer Cell *14*, 471–484.

Christofk, H.R., Vander Heiden, M.G., Harris, M.H., Ramanathan, A., Gerszten, R.E., Wei, R., Fleming, M.D., Schreiber, S.L., and Cantley, L.C. (2008). The M2 splice isoform of pyruvate kinase is important for cancer metabolism and tumour growth. Nature *452*, 230–233.

Dang, C.V. (2009). PKM2 tyrosine phosphorylation and glutamine metabolism signal a different view of the Warburg effect. Sci. Signal. *2*, pe75.

Dang, C.V. (2010). Rethinking the Warburg effect with Myc micromanaging glutamine metabolism. Cancer Res. *70*, 859–862.

Dang, C.V., and Semenza, G.L. (1999). Oncogenic alterations of metabolism. Trends Biochem. Sci. *24*, 68–72.

Day, S.E., Kettunen, M.I., Gallagher, F.A., Hu, D.E., Lerche, M., Wolber, J., Golman, K., Ardenkjaer-Larsen, J.H., and Brindle, K.M. (2007). Detecting tumor response to treatment using hyperpolarized 13C magnetic resonance imaging and spectroscopy. Nat. Med. *13*, 1382–1387.

Fantin, V.R., St-Pierre, J., and Leder, P. (2006). Attenuation of LDH-A expression uncovers a link between glycolysis, mitochondrial physiology, and tumor maintenance. Cancer Cell *9*, 425–434.

Goga, A., Yang, D., Tward, A.D., Morgan, D.O., and Bishop, J.M. (2007). Inhibition of CDK1 as a potential therapy for tumors over-expressing MYC. Nat. Med. *13*, 820–827.

Golman, K., Zandt, R.I., Lerche, M., Pehrson, R., and Ardenkjaer-Larsen, J.H. (2006). Metabolic imaging by hyperpolarized 13C magnetic resonance imaging for in vivo tumor diagnosis. Cancer Res. *66*, 10855–10860.

Harris, T., Eliyahu, G., Frydman, L., and Degani, H. (2009). Kinetics of hyperpolarized 13C1-pyruvate transport and metabolism in living human breast cancer cells. Proc. Natl. Acad. Sci. USA *106*, 18131–18136.

Heber, D., Byerly, L.O., and Chlebowski, R.T. (1985). Metabolic abnormalities in the cancer patient. Cancer ***55*** (1, Suppl), 225–229.

Hu, S., Lustig, M., Balakrishnan, A., Larson, P.E., Bok, R., Kurhanewicz, J., Nelson, S.J., Goga, A., Pauly, J.M., and Vigneron, D.B. (2010). 3D compressed sensing for highly accelerated hyperpolarized (13)C MRSI with in vivo applications to transgenic mouse models of cancer. Magn. Reson. Med. *63*, 312–321.

Kim, J., Lee, J.H., and Iyer, V.R. (2008). Global identification of Myc target genes reveals its direct role in mitochondrial biogenesis and its E-box usage in vivo. PLoS ONE *3*, e1798.

Le, A., Cooper, C.R., Gouw, A.M., Dinavahi, R., Maitra, A., Deck, L.M., Royer, R.E., Vander Jagt, D.L., Semenza, G.L., and Dang, C.V. (2010). Inhibition of lactate dehydrogenase A induces oxidative stress and inhibits tumor progression. Proc. Natl. Acad. Sci. USA *107*, 2037–2042.

Li, F., Wang, Y., Zeller, K.I., Potter, J.J., Wonsey, D.R., O'Donnell, K.A., Kim, J.W., Yustein, J.T., Lee, L.A., and Dang, C.V. (2005). Myc stimulates nuclearly encoded mitochondrial genes and mitochondrial biogenesis. Mol. Cell. Biol. *25*, 6225–6234.

Schindhelm, R.K., Diamant, M., Dekker, J.M., Tushuizen, M.E., Teerlink, T., and Heine, R.J. (2006). Alanine aminotransferase as a marker of non-alcoholic fatty liver disease in relation to type 2 diabetes mellitus and cardiovascular disease. Diabetes Metab. Res. Rev. *22*, 437–443.

Shachaf, C.M., Kopelman, A.M., Arvanitis, C., Karlsson, A., Beer, S., Mandl, S., Bachmann, M.H., Borowsky, A.D., Ruebner, B., Cardiff, R.D., et al. (2004). MYC inactivation uncovers pluripotent differentiation and tumour dormancy in hepatocellular cancer. Nature *431*, 1112–1117.

Shim, H., Dolde, C., Lewis, B.C., Wu, C.S., Dang, G., Jungmann, R.A., Dalla-Favera, R., and Dang, C.V. (1997). c-Myc transactivation of LDH-A: implications for tumor metabolism and growth. Proc. Natl. Acad. Sci. USA *94*, 6658–6663.

Subramanian, A., Tamayo, P., Mootha, V.K., Mukherjee, S., Ebert, B.L., Gillette, M.A., Paulovich, A., Pomeroy, S.L., Golub, T.R., Lander, E.S., and Mesirov, J.P. (2005). Gene set enrichment analysis: a knowledge-based approach for interpreting genome-wide expression profiles. Proc. Natl. Acad. Sci. USA *102*, 15545–15550.

Vander Heiden, M.G., Cantley, L.C., and Thompson, C.B. (2009). Understanding the Warburg effect: the metabolic requirements of cell proliferation. Science *324*, 1029–1033.

Warburg, O. (1956). On respiratory impairment in cancer cells. Science *124*, 269–270.

Wise, D.R., DeBerardinis, R.J., Mancuso, A., Sayed, N., Zhang, X.Y., Pfeiffer, H.K., Nissim, I., Daikhin, E., Yudkoff, M., McMahon, S.B., and Thompson, C.B. (2008). Myc regulates a transcriptional program that stimulates mitochondrial glutaminolysis and leads to glutamine addiction. Proc. Natl. Acad. Sci. USA *105*, 18782–18787.

Yuneva, M., Zamboni, N., Oefner, P., Sachidanandam, R., and Lazebnik, Y. (2007). Deficiency in glutamine but not glucose induces MYC-dependent apoptosis in human cells. J. Cell Biol. *178*, 93–105.